Frontiers in Heat and Mass Transfer

Tech Science Press

DOI: 10.32604/fhmt.2024.056624

ARTICLE

Experimental Analyses of Flow Pattern and Heat Transfer in a Horizontally Oriented Polymer Pulsating Heat Pipe with Merged Liquid Slugs

Zhengyuan Pei[1] **and Yasushi Koito**[2,*]

[1]Department of Mechanical and Mathematical Engineering, Graduate School of Science and Technology, Kumamoto University, Kumamoto, 860-8555, Japan

[2]Division of Industrial Fundamentals, Faculty of Advanced Science and Technology, Kumamoto University, Kumamoto, 860-8555, Japan

*Corresponding Author: Yasushi Koito. Email: koito@gpo.kumamoto-u.ac.jp

Received: 26 July 2024 Accepted: 08 October 2024 Published: 30 October 2024

ABSTRACT

Extended experiments were conducted on the oscillation characteristics of merged liquid slugs in a horizontally oriented polymer pulsating heat pipe (PHP). The PHP's serpentine channel comprised 14 parallel channels with a width of 1.3 mm and a height of 1.1 mm. The evaporator and condenser sections were 25 and 50 mm long, respectively, and the adiabatic section in between was 75 mm long. Using a plastic 3D printer and semi-transparent filament made from acrylonitrile butadiene styrene, the serpentine channel was printed directly onto a thin polycarbonate sheet to form the PHP. The PHP was charged with hydrofluoroether-7100. In the experiments, the evaporator section was heated, and the condenser section was cooled using high-temperature and low-temperature thermostatic baths, respectively. Flow patterns of the working fluid were obtained with temperature distributions of the PHP. A mathematical model was developed to analyze the flow patterns. The merged liquid slugs were observed in every two channels, and their oscillation characteristics were found to be approximately the same in time and space. It was also found that the oscillations of the merged liquid slugs became slower, but the heat transfer rate of the PHP increased with a decrease in the filling ratio of the working fluid. This is because vapor condensation was enhanced in vapor plugs as the filling ratio decreased. However, the filling ratio had a lower limit, and the heat transfer rate was maximum when the filling ratio was 40.6% in the present experimental range.

KEYWORDS

Pulsating heat pipe; polymer heat pipe; visualization experiment; flow pattern analysis; heat transfer enhancement

Nomenclature

A	Amplitude (mm, m), Cross-sectional area (m^2)
c	Specific heat ($J/(kg \cdot K)$)
f	Frequency (Hz)
l	Length (mm, m)
m	Mass (kg)
$\dot{m}$	Mass flow rate (kg/s)

n	Polytropic index
p	Pressure (Pa, kPa)
Q	Heat transfer rate (W)
T	Temperature (°C)
t	Time (s)
V	Filling ratio (%)
v	Velocity (m/s)
y	Coordinate, Position (mm, m)
y_i	Local coordinate, Position (mm, m)

Greek Symbols

Δt	Time difference (ms)
ϕ	Initial phase (rad)
μ	Viscosity (Pa · s)
ω	Angular frequency (rad/s)

Superscripts

0	Initial
I	Condenser side, decreasing
II	Evaporator side, increasing
c	Center

Subscripts

1, 2	Position
a	Adiabatic section
c	Condenser section
e	Evaporator section
i	i th
in	Inlet
LS	Liquid slug
out	Outlet
VP	Vapor plug
w	Cooling water

1 Introduction

The pulsating heat pipe (PHP) is a wickless heat pipe that was invented by Akachi [1] in 1990. The PHP transports heat passively by using a self-induced oscillatory flow of a working fluid, which essentially differs from traditional heat pipes with capillary wick structures (e.g., [2–6]). The PHP is a promising candidate for thermal management, and thus, a great deal of studies have been conducted on the PHP as reviewed in previous articles (e.g., [7–11]). Although the review contents differ between these articles [7–11], they all state that the PHP is a promising candidate for thermal management, especially in electronics cooling. Recently, polymer materials have been used for fabricating the PHPs. As mentioned in our previous papers [12,13], polydimethylsiloxane [14], polyethylene [15], polytetrafluoroethylene [16], and polypropylene [17] were used as the materials of polymer PHPs. In addition, Arai et al. [18] conducted experiments to investigate the heat transfer characteristics of a

polymer PHP, which comprised a polycarbonate serpentine channel and an aluminum plate. The PHP was filled with hydrofluoroether (HFE)-7000 as a working fluid, and the effects of the flow channel size and fill ratio of the working fluid on the PHP's heat transport performance were investigated. Candere et al. [19] proposed the fabrication of a polymer PHP using a common stereolithography technology. FC-72 was used as a working fluid. It was shown that the effective thermal conductivity of the polymer PHP was more than one thousand times higher than the thermal conductivity of a polymer sheet at a 30 W heat input. In our previous study [13], a polymer PHP was made using a 3D printer and filament made from acrylonitrile butadiene styrene (ABS). The PHP was charged with HFE-7100, and the value of 432 $W/(m \cdot K)$ was obtained as the effective thermal conductivity.

Orientation is one of the important factors affecting the thermal performance of the PHPs. Many studies have been conducted in a bottom-heated vertical orientation mode [20–24]. However, it was reported that the thermal performance of the PHPs changed when the orientation was changed from vertical to horizontal. Thompson et al. [25] experimentally investigated the thermal performance of a three-dimensional flat-plate PHP with staggered microchannels using water and acetone as working fluids. It was found that the thermal performance of the PHP in a vertical orientation was better than that in a horizontal orientation. Chien et al. [26] showed that the thermal performance of a copper-water PHP decreased as the PHP's inclination changed from vertical to horizontal. Less orientation dependence was observed for the PHP with dual-diameter channels compared with the PHP with uniform channels. Jun et al. [27] experimentally compared the thermal performance and flow characteristics between closed-loop and closed-end micro-PHPs. The PHP channels were engraved on a silicon wafer using MEMS techniques, and ethanol was employed as a working fluid. It was shown that, in the case of the PHP with 10 and 15 turns, the thermal performance of the closed-loop PHP deteriorated significantly as the PHP's inclination changed from vertical to horizontal. In contrast, the closed-end PHP operated stably regardless of the PHP's inclination. Jung et al. [28] investigated the thermal performance of a PHP with a passive check valve in vertical and horizontal orientations. It was reported that the thermal performance of the PHP in the vertical orientation was better than that in the horizontal orientation. Dixit et al. [29] developed a cryogenic stainless PHP using neon as a working fluid. The lowest thermal resistance of the PHP was 0.17 K/W in a vertical and 0.27 K/W in a horizontal orientation. Although an orientation-independent PHP was reported by Jun et al. [27], many papers describe an orientation-dependent PHP, so orientation is one of the important factors to consider when developing PHPs.

The above-mentioned ABS PHP using HFE-7100 was also affected by the orientation. That is, differing from flow patterns in a vertical orientation, an oscillatory flow of merged liquid slugs was observed in a horizontal orientation [30]. This is a unique characteristic of the ABS PHP, but the details have not been discussed. Because of this, extended experiments were conducted in the present study regarding the oscillation characteristics of the merged liquid slugs in the horizontally oriented PHP. A semi-transparent ABS PHP was employed with HFE-7100. Flow patterns of the merged liquid slugs were obtained along with temperature distributions of the PHP. A mathematical model was developed to analyze the flow patterns. The oscillation characteristics were discussed based on the analytical results of the flow patterns. Discussion was also conducted on the effect of the filling ratio of the working fluid on the oscillation and the heat transfer characteristics of the PHP.

2 Experimental Methods

Fig. 1 shows a schematic diagram of the PHP. This is the same PHP as in our previous study [13], in which experiments were conducted in a vertical orientation mode. Because the design and

fabrication method of the PHP including 3D printing and material selection were already described in our previous paper [13], only their brief overview is presented here. As shown in Fig. 1a, a serpentine channel of the PHP comprised 14 parallel channels with a width of 1.3 mm and a height of 1.1 mm. The serpentine channel was made by using a plastic 3D printer; semi-transparent ABS filament was used as a 3D printing material. The fused filament fabrication 3D printing technique was employed. This technique causes some unevenness on the 3D printed surface, but the unevenness was less than 0.1 mm high, which is acceptable for this study. As shown in Fig. 1b, the ABS serpentine channel was printed directly onto a polycarbonate sheet to form the PHP. The polycarbonate sheet was 0.12 mm thick and was used to reduce the conductive thermal resistance of the PHP wall. The outer surface of the PHP was chemically treated to maintain airtightness. The evaporator and condenser sections were 25 and 50 mm long, respectively, and the adiabatic section in between was 75 mm long.

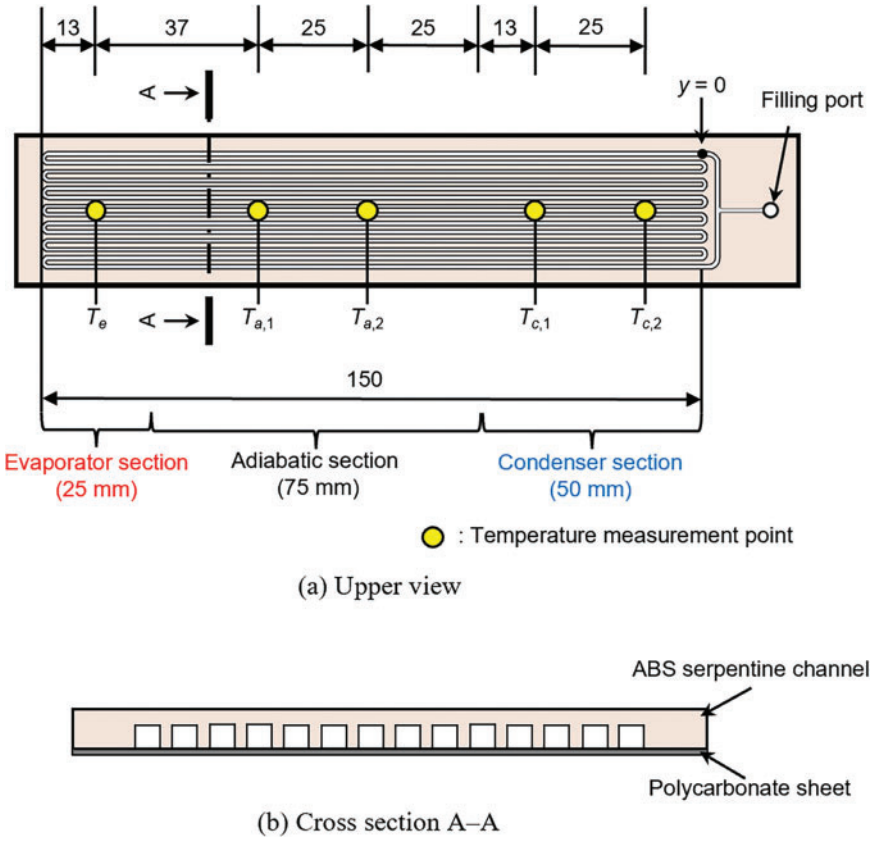

Figure 1: Schematic diagram of the PHP (unit: mm)

Fig. 2 shows a schematic diagram of the experimental apparatus. Heating and cooling jackets were mounted at the evaporator and condenser sections, respectively, of the PHP on the polycarbonate sheet side. Thermal grease was used between the polycarbonate sheet and the jackets. The heating and cooling jackets were piped to high-temperature and low-temperature thermostatic baths, respectively. A vacuum pump and a pressure transducer were employed to evacuate air from inside the PHP. A high-speed camera was placed above the PHP with lighting devices; fluid flow phenomena in the PHP were captured through the semi-transparent ABS wall of the serpentine channel. Except for the heated and cooled sections, the rest of the PHP was covered with a thermal insulation material to reduce heat

loss. Figs. 1 and 2 also show temperature measurement points. T-type thermocouples were attached at the evaporator (T_e), adiabatic ($T_{a,1}$, $T_{a,2}$), and condenser ($T_{c,1}$, $T_{c,2}$) sections on the surface of the PHP on the polycarbonate sheet side. Small grooves with the same depth as the diameter of the thermocouples were made between the PHP and the jackets, and the thermocouples for T_e, $T_{c,1}$, and $T_{c,2}$ were installed. The temperatures at the inlet ($T_{w,in}$) and outlet ($T_{w,out}$) of the cooling jacket were also measured by using T-type thermocouples, and the heat transfer rate (Q) of the PHP was evaluated by

$$Q = \dot{m}c(T_{w,out} - T_{w,in}) \tag{1}$$

where $\dot{m}$ is the mass flow rate and c is the specific heat of the cooling water. To obtain the $\dot{m}$ value, a flow meter was set in a pipe between the cooling jacket and the low-temperature thermostatic bath.

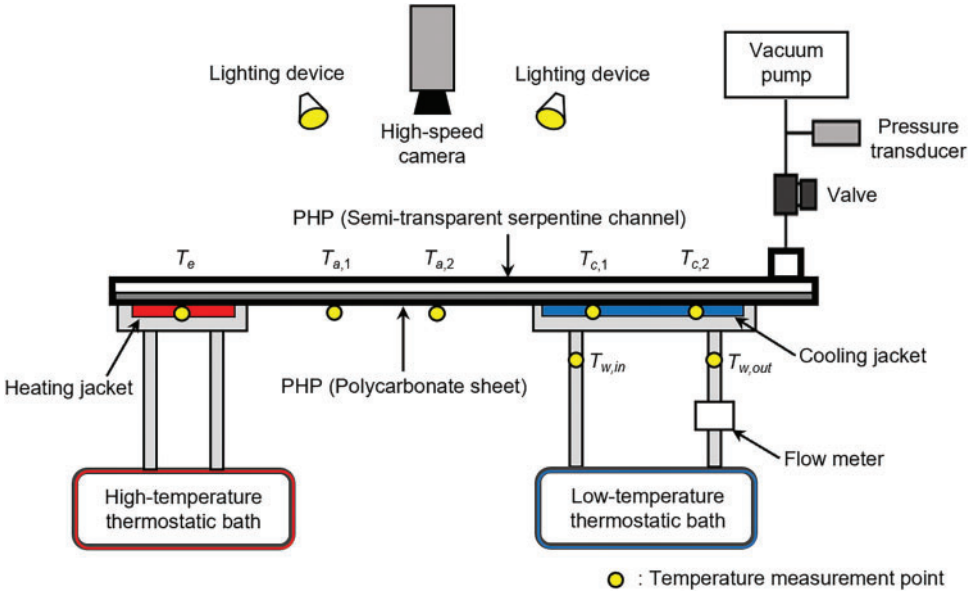

Figure 2: Schematic diagram of the experimental apparatus

The PHP was charged with HFE-7100. The representative physical properties of HFE-7100 were shown in the previous paper [31]. Fig. 3 shows schematic diagrams of working fluid distribution states in the PHP. The working fluid was distributed in the form of liquid slugs and vapor plugs, which are shown by using dark and light colors, respectively. Fig. 3a is a distribution state immediately after filling the PHP with the working fluid. Liquid slugs and vapor plugs were well distributed throughout the PHP channel. However, this distribution was greatly affected by gravity [30]. That is, when the PHP was oriented vertically, the liquid slugs flowed down, and the vapor plugs flowed up resulting in a distribution state where the liquid slugs and vapor plugs were completely separated. The PHP channel was designed based on the Bond number, which is the ratio of gravitational force to surface tension force. When the working fluid was changed from HFE-7100 to water, a well-distributed state like Fig. 3a was maintained under the same Bond number, which implies that the influence of the gravitational force was different between HFE-7100 and water. The influence was significant for HFE-7100, and thus unique oscillation characteristics of merged liquid slugs were observed in the present PHP. From the distribution state of Fig. 3a, the liquid volumes in each PHP channel were adjusted by tilting the PHP forward, backward, left, and right so that the lengths of all long liquid slugs were approximately the same. Thereafter, the PHP was oriented horizontally, and the distribution state shown in Fig. 3b was obtained. Long liquid slugs were located on the condenser side while the

evaporator side was occupied by long vapor plugs. The experiment was started from this distribution state. The cooling jacket was cooled with cooling water, and then heating water was supplied to the heating jacket. Immediately after that, the PHP was tilted slightly for a short time, which started the oscillations of long liquid slugs and long vapor plugs, and the distribution state shown in Fig. 3c was obtained. The heating and cooling were conducted at approximately $T_e = 90°C$, $T_{w,in} = 10°C$, and $\dot{m} = 100$ g/ min, and temperatures $T_{a,1}$, $T_{a,2}$, $T_{c,1}$, $T_{c,2}$, and $T_{w,out}$ were obtained at a pseudo steady state. In addition, the oscillation phenomena were captured using a high-speed camera with 1000 fps. The experiments were conducted by varying the filling ratio of the working fluid (V) as 37.1%, 40.6%, 52.0%, 62.9%, and 69.2%. The filling ratio was defined as the ratio of the liquid volume to the inner volume of the serpentine channel.

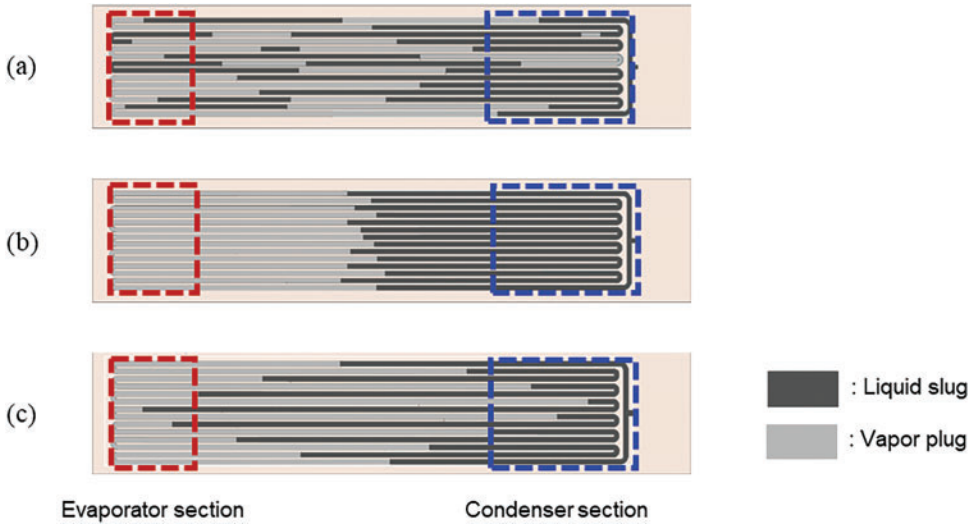

Figure 3: Schematic diagrams of working-fluid distribution states (a: distribution state immediately after filling the PHP with the working fluid, b: distribution state just before starting the experiment, c: distribution state when the PHP is operating)

3 Results and Discussion

3.1 Fluid Flow Characteristics

Fig. 4 shows flow patterns in all channels of the PHP when the filling ratio (V) was 62.9%, the heating temperature (T_e) was 89.2°C, and the cooling temperature ($T_{w,in}$) was 10.0°C. The vertical axis is the coordinate (y) along the serpentine channel. $y = 0$ is shown in Fig. 1. Dashed lines indicate the divisions of each channel. Evaporator, adiabatic, and condenser sections are indicated by using red, green, and blue colors, respectively. The flow patterns were obtained by analyzing the oscillation phenomena captured with a high-speed camera. Video analysis software was used for the analysis. The process to obtain the flow patterns from images captured with a high-speed camera was explained in our previous paper [12]. Liquid slugs are shown in the dark while light colors imply vapor plugs. Although the flow patterns are not completely binarized, the oscillation characteristics of liquid slugs and vapor plugs can be evaluated by the shade of color. Because liquid slugs merged as shown in Fig. 3, long liquid slugs were found in every two channels, and their periodic oscillations were observed on the condenser side; the rest of the channels were occupied by long vapor plugs. Because of the periodic oscillations in every two channels, the serpentine channel was divided into subchannels of *Ch*. 1 to

Ch. 6 as shown in Fig. 4. In addition, the long liquid slugs and long vapor plugs were numbered *LS*-1 to *LS*-6 and *VP*-1 to *VP*-7, respectively. Fig. 5 is an enlarged view of Fig. 4, where the flow patterns in *Ch*. 4 and 5 are shown. For flow pattern analysis, local coordinates (y_i) were set from the end of each subchannel, and the positions of vapor-liquid interfaces of i th long liquid slug (*LS*-i) on the condenser and evaporator side were denoted by y_i^{I} and y_i^{II}, respectively. y_4, y_4^{I}, y_4^{II}, and y_5, y_5^{I}, y_5^{II} are shown in Fig. 5. In addition, the frequency and the time difference of *LS*-i were denoted by f_i and Δt_i, respectively. Note that Δt_i was defined by a time difference between i th and $i+1$ th long liquid slugs.

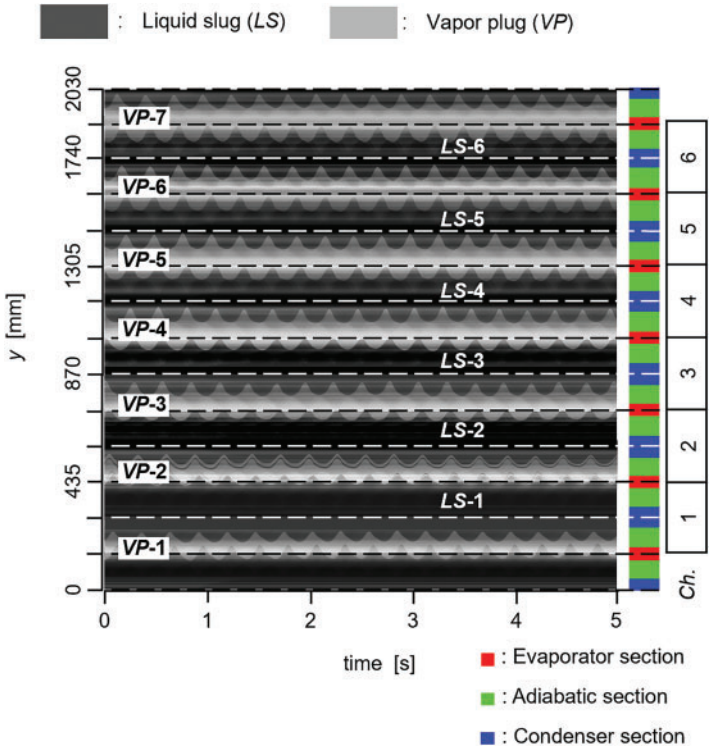

Figure 4: Flow patterns in all channels of the PHP ($V = 62.9\%$, $T_e = 89.2^{\circ}$C, $T_{w,in} = 10.0^{\circ}$C, $Q = 8.13$ W)

Fig. 6 shows the y_i^{I}, y_i^{II}, f_i, and Δt_i values for *LS*-1 to *LS*-6. These values were obtained from the flow patterns in Fig. 4. Because of oscillations, the y_i^{I} and y_i^{II} values changed with time; thus, the average values of y_i^{I} and y_i^{II} are shown by symbols with bars indicating their variation ranges. As indicated by gray thick bars, the region between y_i^{I} and y_i^{II} corresponds to a long liquid slug. Before starting the experiment, the liquid volumes in each PHP channel were adjusted as mentioned earlier. However, it was very difficult to distribute the working fluid evenly throughout the entire serpentine channel; thus, slight differences were found in the length ($y_i^{\mathrm{II}} - y_i^{\mathrm{I}}$) of long liquid slugs. Nevertheless, it was found that the f_i and Δt_i values for all long liquid slugs were approximately the same. In addition, all long liquid slugs were oscillating in the same range, that is, y_i^{I} was oscillating between the condenser and adiabatic sections, and y_i^{II} was between the adiabatic and evaporator sections. These findings confirmed that the oscillation characteristics of the long liquid slugs were essentially the same in time and space.

The average values of f_i and Δt_i were 3.62 Hz and 39.2 ms, respectively. When the average oscillation period ($1/f_i$) was divided by the number of subchannels including an end channel, we obtained the value of 39.5 ms, which was found to be close to the average value of Δt_i.

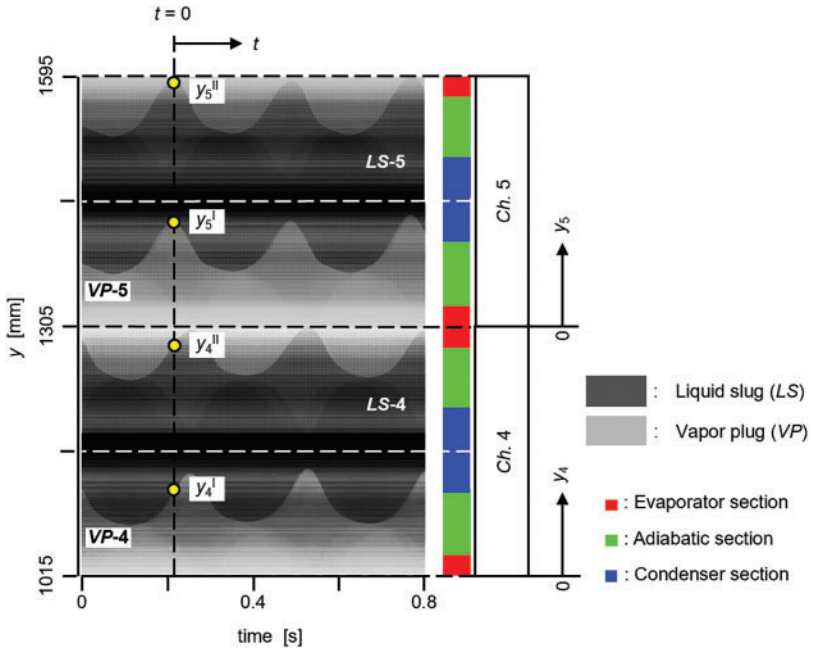

Figure 5: Enlarged view of the flow patterns in *Ch.* 4 and 5 ($V = 62.9\%$, $T_e = 89.2°C$, $T_{w,in} = 10.0°C$, $Q = 8.13$ W)

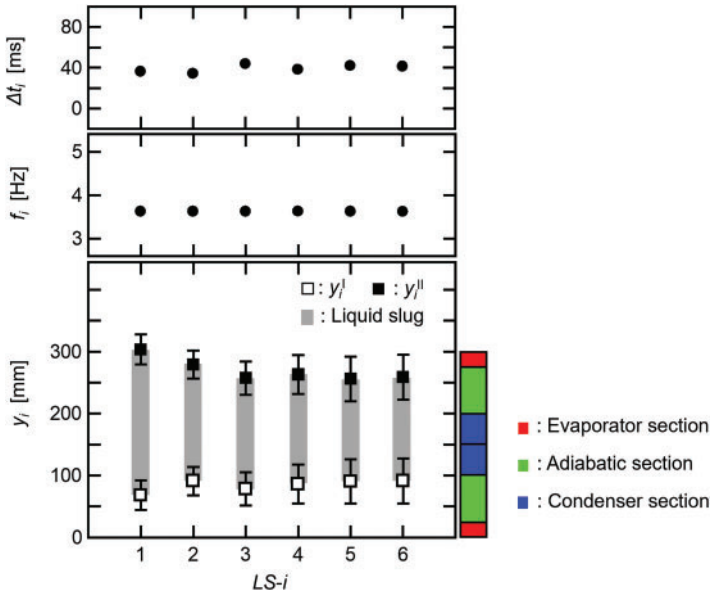

Figure 6: Oscillation characteristics of the long liquid slugs (*LS*-1 to *LS*-6, $V = 62.9\%$, $T_e = 89.2°C$, $T_{w,in} = 10.0°C$, $Q = 8.13$ W)

3.2 Flow Pattern Analyses

For *VP*-5 in Fig. 5, the temporal change in the length of *VP*-5 ($l_{VP\text{-}5}$) was obtained as shown in Fig. 7. Fig. 7a is the flow pattern of *VP*-5, and Fig. 7b shows the change in $l_{VP\text{-}5}$. Because of the

periodicity, the change only in one period is shown, and $t = 0$ was set at the time when $l_{VP\text{-}5}$ was maximum. $t = 0$ is also shown in Fig. 5. Fig. 7a indicates that the vapor-liquid interface of *VP*-5 on the *LS*-5 side was oscillating across the boundary (blue dashed line) between the condenser and adiabatic sections, while the vapor-liquid interface on the *LS*-4 side across the boundary (red dashed line) between the adiabatic and evaporator sections. Thus, based on the crossing points (yellow symbols) when the vapor-liquid interfaces crossed the boundaries, the one period was divided into four subperiods of *SP-a*, *b*, *c*, and *d* as shown in Fig. 7a. It was assumed that evaporation of liquid occurred when the vapor-liquid interface was in the evaporator section, and condensation of vapor occurred when the interface was in the condenser section. Based on these assumptions, the four subperiods were characterized as follows: evaporation and condensation occurred in *SP-a*, only evaporation in *SP-b*, no evaporation and no condensation in *SP-c*, and only condensation in *SP-d*. The four subperiods are also shown in Fig. 7b. Because of the phase difference between oscillating *LS*-4 and *LS*-5, $l_{VP\text{-}5}$ decreased and then increased in one period. The change in $l_{VP\text{-}5}$ was greater when it was decreasing than when increasing. Moreover, in Fig. 7b, *SP-b* is shown when $l_{VP\text{-}5}$ was decreasing, and *SP-d* is shown when $l_{VP\text{-}5}$ was increasing, which implies that only evaporation occurred when *VP-5* was compressed, and only condensation occurred when *VP-5* was expanding. These evaporation and condensation characteristics would increase and decrease the vapor pressure in *VP*-5 effectively, which continued the periodic oscillations of long liquid slugs.

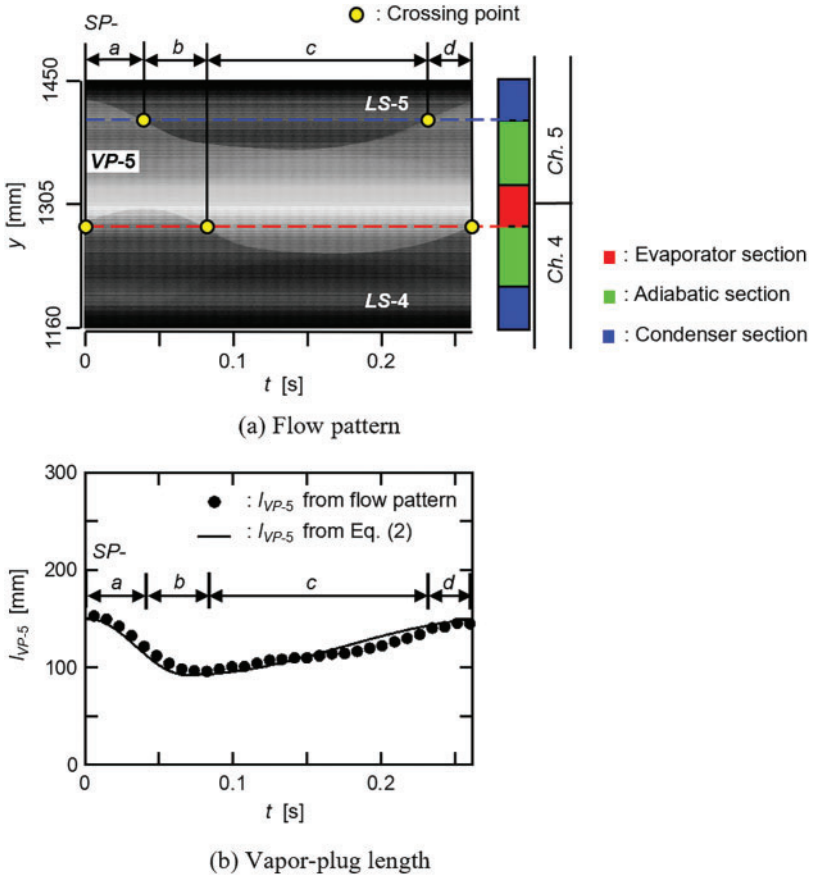

Figure 7: Temporal change in the vapor-plug length (*VP*-5, $V = 62.9\%$, $T_e = 89.2^{\circ}$C, $T_{w,in} = 10.0^{\circ}$C, $Q = 8.13$ W)

The following empirical equation was proposed to express the length of i th long vapor plug (l_{VP-i}) as a function of t:

$$l_{VP-i} = A_{VP-i} \cos\left(\omega_{VP-i} t + \phi_{VP-i}\right) \tag{2}$$

where A_{VP-i} is the amplitude, ω_{VP-i} is the angular frequency, and ϕ_{VP-i} is the initial phase. Because the change rate of l_{VP-i} was different when it was decreasing and increasing, two angular frequencies ($\omega^{\mathrm{I}}_{VP-i}$, $\omega^{\mathrm{II}}_{VP-i}$) were used, and ω_{VP-i} was given by

$$\left.\begin{array}{ll} \omega_{VP-i} = \omega^{\mathrm{I}}_{VP-i} & \text{when } l_{VP-i} \text{ is decreasing} \\ \omega_{VP-i} = \omega^{\mathrm{II}}_{VP-i} & \text{when } l_{VP-i} \text{ is increasing} \end{array}\right\} \tag{3}$$

The values of the four constants (A_{VP-i}, $\omega^{\mathrm{I}}_{VP-i}$, $\omega^{\mathrm{II}}_{VP-i}$, ϕ_{VP-i}) can be obtained by fitting Eq. (2) to the l_{VP-i} values obtained from the flow pattern. For VP-5, $A_{VP-5} = 34.7$ mm, $\omega^{\mathrm{I}}_{VP-5} = 41.9$ rad/s, $\omega^{\mathrm{II}}_{VP-5} = 17.3$ rad/s, and $\phi_{VP-5} = 1.57$ rad were obtained, and Eq. (2) for l_{VP-5} is also shown in Fig. 7. A good agreement with l_{VP-5} from the flow pattern confirmed the validity of the empirical equation of Eq. (2).

For the i th long liquid slug, the equation of motion is expressed as

$$m_{LS-i} \frac{d^2 y^c_i}{dt^2} = \left(p_{VP-i} - p_{VP-(i+1)}\right) A_{LS-i} - 8\pi \mu_{LS-i} l_{LS-i} \frac{dy^c_i}{dt} \tag{4}$$

where m_{LS-i}, A_{LS-i}, μ_{LS-i}, and l_{LS-i} are the mass, cross-sectional area, viscosity, and length of LS-i, respectively. y^c_i is the center position of LS-i in the local coordinate. p_{VP-i} and $p_{VP-(i+1)}$ are the vapor pressures in the i and $i+1$ th long vapor plugs, respectively. The last term on the right side of Eq. (4) is the force due to friction, which was considered according to the literature [32]. Initial conditions were given by

$$\left.\begin{array}{ll} y^c_i = y^{c,0}_i & \text{at } t = 0 \\ \dfrac{dy^c_i}{dt} = v^0_i & \text{at } t = 0 \end{array}\right\} \tag{5}$$

When the same polytropic change was assumed for the i and $i+1$ th long vapor plugs, Eq. (6) was obtained.

$$p_{VP-i} \left(l_{VP-i}\right)^n = p_{VP-(i+1)} \left(l_{VP-(i+1)}\right)^n = p^0_{VP-i} \left(l^0_{VP-i}\right)^n \tag{6}$$

where n is the polytropic index. p^0_{VP-i} and l^0_{VP-i} are the initial pressure and initial length of VP-i, respectively. The p^0_{VP-i} and l^0_{VP-i} values were obtained from the experimental conditions, and the $y^{c,0}_i$ and v^0_i values were obtained from the flow patterns. In addition, Eq. (2) was used to calculate l_{VP-i} and $l_{VP-(i+1)}$, and then the n value was obtained by fitting the y^c_i value numerically calculated from Eqs. (4)–(6) to that obtained from the flow pattern. For LS-4, $y^{c,0}_4 = 171$ mm, $v^0_4 = 0.605$ m/s, $p^0_{VP-4} = 76.1$ kPa, $l^0_{VP-4} = 0.189$ m, and $n = 0.295$ were obtained with the fitting result shown in Fig. 8. Although a slight difference was found in the fitting, the y^c_4 value from Eqs. (4)–(6) was in good agreement with that from the flow pattern. Therefore, Eqs. (4)–(6) can be used for further analyses of the flow patterns.

From Eqs. (4)–(6), temporal changes in the net force acting on LS-4 and the velocity of LS-4 were numerically obtained as shown in Fig. 9a,b, respectively. The net force was expressed by the right side of Eq. (4), and the numerical result was also shown in Fig. 9a when the frictional force was neglected in Eq. (4). The frictional force acts in the opposite direction to the velocity, and thus the net force with the frictional force was less than that without the frictional force when the velocity was positive.

Conversely, the net force with the frictional force was greater than that without the frictional force when the velocity was negative. Since a difference was found between the two net forces, the frictional force was considered in Eq. (4).

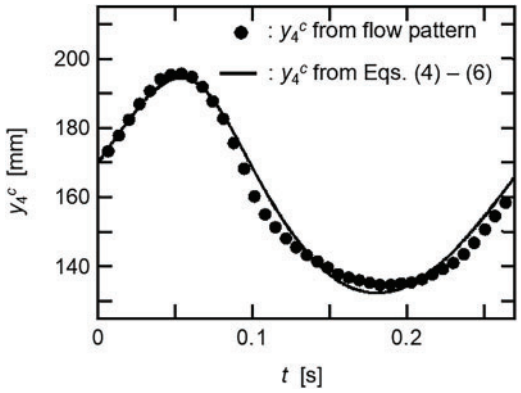

Figure 8: Comparison between the liquid-slug positions obtained from flow pattern and Eqs. (4)–(6) (*LS*-4, $V = 62.9\%$, $T_e = 89.2°C$, $T_{w,in} = 10.0°C$, $Q = 8.13$ W)

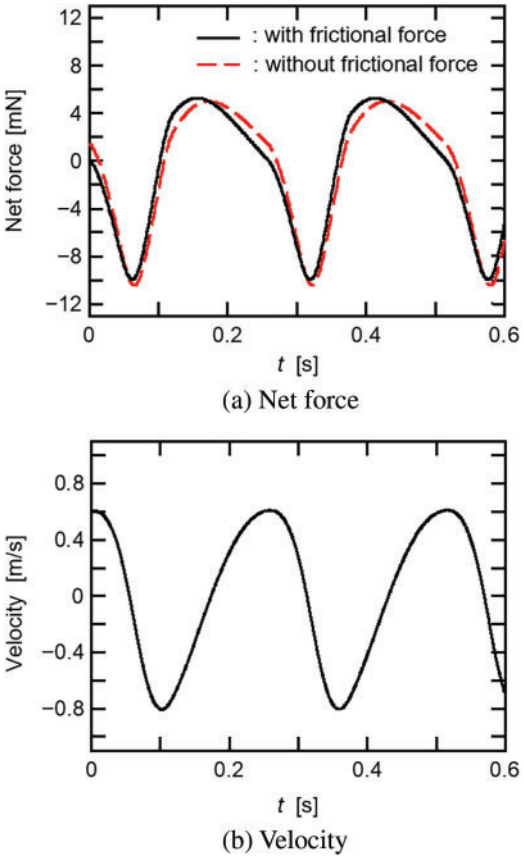

Figure 9: Effect of the frictional force on the net force and velocity of the long liquid slug (*LS*-4, $V = 62.9\%$, $T_e = 89.2°C$, $T_{w,in} = 10.0°C$, $Q = 8.13$ W)

3.3 Effect of Filling Ratio

Fig. 10 shows the oscillation characteristics of a long liquid slug when the filling ratio (V) was changed. Although V was changed, long liquid slugs were observed in every two channels, and their oscillation characteristics were found to be approximately the same in time and space. Thus, the flow patterns for LS-4 were analyzed at each V, and the y_4^{I}, y_4^{II}, f_4, and Δt_4 values are shown for $V = 40.6\%$, 52.0%, 62.9%, and 69.2%. In addition, y_5^{I} is also shown in the figure. Like Fig. 6, the average values of y_4^{I}, y_4^{II}, and y_5^{I} are shown by symbols with bars indicating their variation ranges. Gray thick bars between y_4^{I} and y_4^{II} correspond to LS-4, and hatched thick bars between y_4^{II} and y_5^{I} mean VP-5. As expected, the length $(y_4^{\mathrm{II}} - y_4^{\mathrm{I}})$ of LS-4 became shorter while the length $(y_5^{\mathrm{I}} - y_4^{\mathrm{II}})$ of VP-5 became longer as V decreased. However, the influence of V was mainly found for the vapor-liquid interfaces on the condenser side. That is, y_4^{I} and y_5^{I} increased with decreasing V while the change in y_4^{II} was very small. Long vapor plugs mainly extended toward the condenser side as V decreased. Fig. 10 also showed that f_4 decreased while Δt_4 increased with decreasing V.

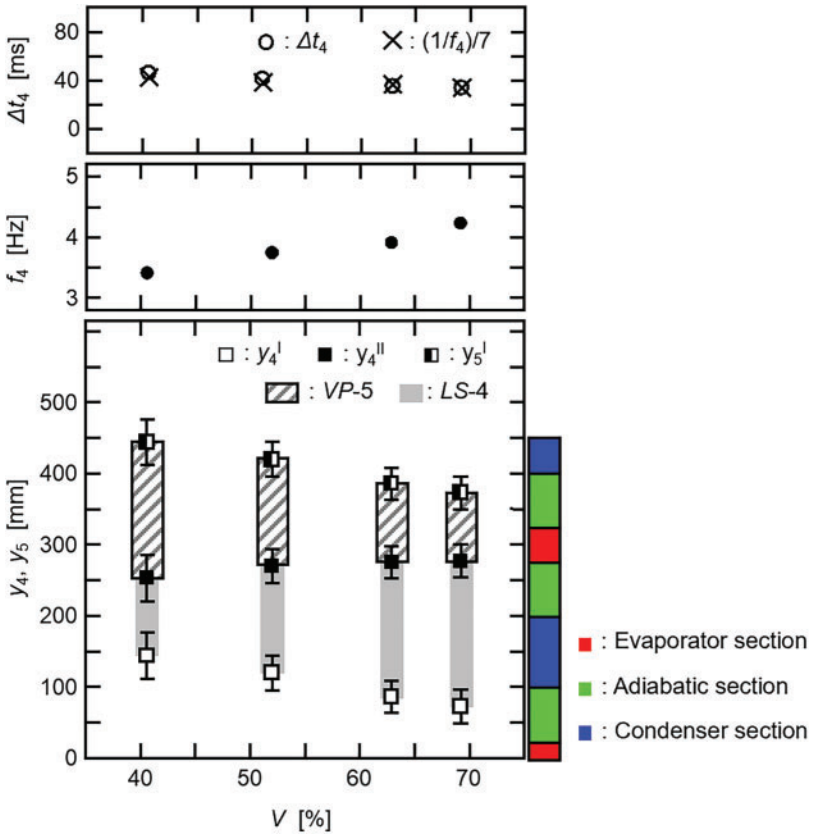

Figure 10: Effect of the filling ratio on the oscillation characteristics of the long liquid slug (LS-4)

For $V = 40.6\%$, 52.0%, 62.9%, and 69.2%, temporal changes in the net force acting on LS-4 and the velocity of LS-4 were numerically obtained from Eqs. (4)–(6), and the numerical results are shown in Fig. 11a,b, respectively. The $y_4^{c,0}$, v_4^0, p_{VP-4}^0, l_{VP-4}^0, and n values were obtained from each experiment condition and flow pattern. Fig. 11a indicates that the change rate of the net force and its fluctuation range became smaller with decreasing V. Although the mass of LS-4 was reduced, the fluctuations were mitigated with decreasing V. As mentioned earlier, the long vapor plugs mainly extended toward

the condenser side as V decreased. Since this extension increased the condensation surface area, the condensation of vapor was enhanced in the long vapor plugs as V decreased. Because of this, the fluctuations of the net force were mitigated with decreasing V. Moreover, the mass of the long liquid slugs was reduced with decreasing V. Thus, as shown in Fig. 11b, the effect of V on the fluctuation range of the velocity was smaller than that of the net force. Fig. 11b also indicates that V mainly affected the change rate of the velocity, and thus, because of a decrease in the change rate, f_4 decreased with decreasing V. In Fig. 10, Δt_4 is compared with the value of $(1/f_4)/7$, which implies that the oscillation period $(1/f_4)$ was divided by the number of subchannels including an end channel. The comparison showed a close agreement, which confirmed that Δt_4 was inversely proportional to f_4, and increased with decreasing V.

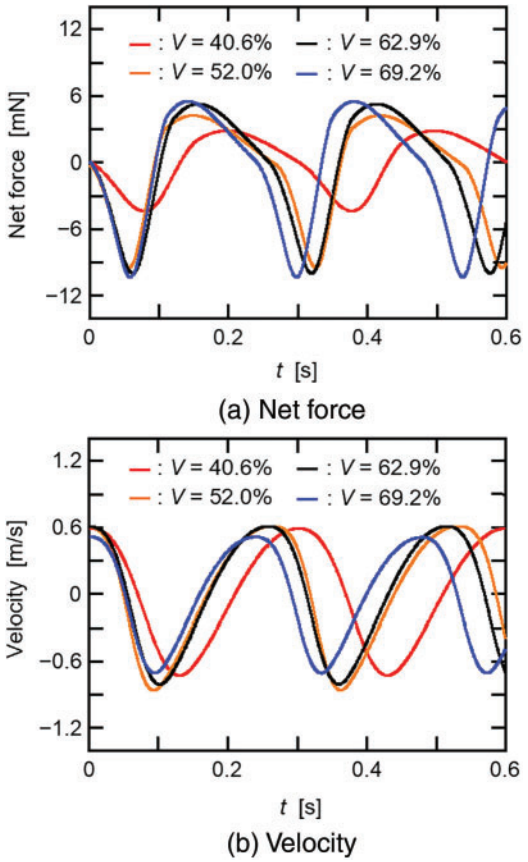

Figure 11: Effect of the filling ratio on the net force and velocity of the long liquid slug (*LS*-4)

Table 1 shows the heat transfer rate (Q) of the PHP at different V. The Q value was obtained from the experimental results using Eq. (1). Heat is transferred from the evaporator section to the condenser section through long vapor plugs. This heat transfer rate was increased by the above-mentioned enhancement of condensation in the long vapor plugs, and thus the Q value increased with decreasing V from $V = 69.2\%$ to $V = 40.6\%$. However, when V was 37.1%, continuous oscillations of the long liquid slugs and long vapor plugs were not obtained. Thus, V had a lower limit, and Q was maximum at $V = 40.6\%$ in the present experimental range. In a vertically oriented PHP [12], the heat transfer was enhanced by the occurrence of a circulation flow, which is a vapor-liquid two-phase

flow in one direction. Because of no circulation flow, the thermal performance of the present PHP in a horizontal orientation was lower than that in a vertical orientation.

Table 1: Effect of the filling ratio on the heat transfer rate of the PHP

V (%)	Q (W)
37.1 ($T_e = 91.5$°C, $T_{w,in} = 10.4$°C, $\dot{m} = 98$ g/min)	No continuous operation
40.6 ($T_e = 90.0$°C, $T_{w,in} = 10.4$°C, $\dot{m} = 102$ g/min)	11.0
52.0 ($T_e = 90.9$°C, $T_{w,in} = 10.1$°C, $\dot{m} = 104$ g/min)	9.50
62.9 ($T_e = 89.2$°C, $T_{w,in} = 10.0$°C, $\dot{m} = 106$ g/min)	8.13
69.2 ($T_e = 90.1$°C, $T_{w,in} = 10.0$°C, $\dot{m} = 103$ g/min)	7.01

4 Conclusions

Extended experiments were conducted on the oscillation characteristics of merged liquid slugs in the horizontally oriented polymer PHP with HFE-7100 working fluid. Flow patterns of merged liquid slugs were obtained and then numerically analyzed. The oscillation and heat transfer characteristics at different filling ratios of the working fluid were discussed. The findings are summarized as follows:

- Merged liquid slugs were observed in every two channels, and their oscillation characteristics were found to be approximately the same in time and space.
- The mathematical model was developed on the oscillation characteristics of the merged liquid slug. This model was effective in analyzing the flow patterns.
- Because the condensation of vapor was enhanced in vapor plugs, the oscillations of the merged liquid slugs became slower with a decrease in the filling ratio of the working fluid.
- Heat is transferred from the evaporator section to the condenser section through the vapor plugs. This heat transfer rate was increased by the above-mentioned enhancement of condensation in the vapor plugs, and thus the heat transfer rate of the PHP increased with a decrease in the filling ratio.
- However, the filling ratio had a lower limit, and the heat transfer rate was maximum when the filling ratio was 40.6% in the present experimental range.
- Because of no circulation flow, the thermal performance of the PHP in a horizontal orientation was lower than that in a vertical orientation.

It is considered that the present PHP would be affected by many factors such as the number and size of the PHP channel, and the heating and cooling conditions. Our next step is to examine the influences of these factors. In addition, the influences of gravitational force and surface tension force on the PHP operation are different between the two kinds of working fluids: HFE-7100 and water. Thus, an extended analysis is also a future work to clarify the reason for this difference.

Acknowledgement: The authors thank N. Nagasato, A. Yang, S. Okubo, and Y. Sugano for their help in conducting the experiments.

Funding Statement: This work was supported by JSPS KAKENHI Grant Number 22K03947.

Author Contributions: The authors confirm contribution to the paper as follows: study conception and design: Zhengyuan Pei, Yasushi Koito; data collection: Zhengyuan Pei; analysis and interpretation of results: Zhengyuan Pei, Yasushi Koito; draft manuscript preparation: Zhengyuan Pei, Yasushi Koito. All authors reviewed the results and approved the final version of the manuscript.

Availability of Data and Materials: The data are available from the corresponding author upon reasonable request.

Ethics Approval: Not applicable.

Conflicts of Interest: The authors declare that they have no conflicts of interest to report regarding the present study.

References

1. Akachi H. Structures of a heat pipe. U.S. Patent. 1990;4921041.
2. Yin L, Liu H, Liu W. Capillary character and evaporation heat transfer in the wicks of high temperature liquid metal heat pipe. Appl Therm Eng. 2020;175:115284. doi:10.1016/j.applthermaleng.2020.115284.
3. Saygan S, Akkus Y, Dursunkaya Z, Cetin B. Capillary boosting for enhanced heat pipe performance through bifurcation of grooves: numerical assessment and experimental validation. Int Commun Heat Mass Transf. 2022;137:106162. doi:10.1016/j.icheatmasstransfer.2022.106162.
4. Ma Y, Wang X, Yu H, Huang S, Zhang Y, Su GH, et al. Capillary limit of a sodium screen-wick heat pipe. Appl Therm Eng. 2023;232:120972. doi:10.1016/j.applthermaleng.2023.120972.
5. Zhou Z, Wu B, Zhu L, Lu J, Cheng T, Tang Y, et al. Enhanced the capillary performance of the injection molded flexible heat pipe shell by the composite microgroove wicks. Therm Sci Eng Prog. 2024;51:102656. doi:10.1016/j.tsep.2024.102656.
6. Elkholy A, Narvan M, Thompson S, Durfee J, Kempers R. The effect of layer thickness on the geometry and capillary performance of strut-based heat pipe wicks manufactured by laser powder bed fusion. Int J Thermofluids. 2024;21:100543. doi:10.1016/j.ijft.2023.100543.
7. Nazari MA, Ahmadi MH, Ghasempour R, Shafii MB. How to improve the thermal performance of pulsating heat pipes: a review on working fluid. Renew Sust Energ Rev. 2018;91:630–8. doi:10.1016/j.rser.2018.04.042.
8. Bastakoti D, Zhang H, Li D, Cai W, Li F. An overview on the developing trend of pulsating heat pipe and its performance. Appl Therm Eng. 2018;141:305–32. doi:10.1016/j.applthermaleng.2018.05.121.
9. Xu Y, Xue Y, Qi H, Cai W. An updated review on working fluids, operation mechanisms, and applications of pulsating heat pipes. Renew Sust Energ Rev. 2021;144:110995. doi:10.1016/j.rser.2021.110995.
10. Su Z, Hu Y, Zheng S, Wu T, Liu K, Zhu M, et al. Recent advances in visualization of pulsating heat pipes: a review. Appl Therm Eng. 2023;221:119867. doi:10.1016/j.applthermaleng.2022.119867.
11. Fazli M, Mehrjardi SAA, Mahmoudi A, Khademi A, Amini M. Advancements in pulsating heat pipes: exploring channel geometry and characteristics for enhanced thermal performance. Int J Thermofluids. 2024;22:100644. doi:10.1016/j.ijft.2024.100644.
12. Nagasato N, Pei Z, Koito Y. Flow patterns and heat transfer characteristics of a polymer pulsating heat pipe filled with hydrofluoroether. Front Heat Mass Transf. 2024;22(1):49–63. doi:10.32604/fhmt.2024.047502.
13. Koito Y, Yoshida H, Pei Z. An experimental study of a polymer pulsating heat pipe 3D-printed on a thin polymer sheet. Multiphase Sci Technol. 2021;33(4):31–43. doi:10.1615/MultScienTechn.v33.i4.
14. Lin Y, Kang S, Wu T. Fabrication of polydimethylsiloxane (PDMS) pulsating heat pipe. Appl Therm Eng. 2009;29(2–3):573–80.

15. Lim J, Kim SJ. Fabrication and experimental evaluation of a polymer-based flexible pulsating heat pipe. Energy Convers Manag. 2018;156:358–64. doi:10.1016/j.enconman.2017.11.022.
16. Hao T, Ma H, Ma X. Heat transfer performance of polytetrafluoroethylene oscillating heat pipe with water, ethanol, and acetone as working fluids. Int J Heat Mass Transf. 2019;131(11–12):109–20. doi:10.1016/j.ijheatmasstransfer.2018.08.133.
17. Der O, Alqahtani AA, Marengo M, Bertola V. Characterization of polypropylene pulsating heat stripes: effects of orientation, heat transfer fluid, and loop geometry. Appl Therm Eng. 2021;184(19):116304. doi:10.1016/j.applthermaleng.2020.116304.
18. Arai T, Kawaji M. Thermal performance and flow characteristics in additive manufactured polycarbonate pulsating heat pipes with Novec 7000. Appl Therm Eng. 2021;197(2):117273. doi:10.1016/j.applthermaleng.2021.117273.
19. Candere AC, Miché N, Bernagozzi M, Saglam M, Georgoulas A, Aydin O, et al. A novel fabrication method for polymeric flat plate pulsating heat pipe via additive manufacturing. Appl Therm Eng. 2024;241:122398. doi:10.1016/j.applthermaleng.2024.122398.
20. Kim J, Kim SJ. Experimental investigation on working fluid selection in a micro pulsating heat pipe. Energy Convers Manag. 2020;205:112462. doi:10.1016/j.enconman.2019.112462.
21. Min C, Gao X, Li F, Wang K. Thermal performance analyses of pulsating heat pipe for application in proton exchange member fuel cell. Energy Convers Manag. 2022;259(1–2):115566. doi:10.1016/j.enconman.2022.115566.
22. Malla LK, Vempeny DT, Dileep H, Dhanalakota P, Mahapatra PS, Srivastava P, et al. Thermal performance comparison of flat plate pulsating heat pipes of different material thermal conductivity using ethanol-water mixtures. Appl Therm Eng. 2024;236:121475. doi:10.1016/j.applthermaleng.2023.121475.
23. Chen X, Li H, Han X, Liu X. Thermo-hydrodynamic characteristics of a novel flat-plate micro pulsating heat pipe with asymmetric converging-diverging channels. Int Commun Heat Mass Transf. 2024;152(4):107282. doi:10.1016/j.icheatmasstransfer.2024.107282.
24. Wang Z, Fan Y, Zhang Y, Lai Z. Chaotic index analysis of ethanol-based graphene nanofluid pulsating heat pipe. Appl Therm Eng. 2024;236:121870. doi:10.1016/j.applthermaleng.2023.121870.
25. Thompson SM, Cheng P, Ma HB. An experimental investigation of a three-dimensional flat-plate oscillating heat pipe with staggered microchannels. Int J Heat Mass Transf. 2011;54(17–18):3951–9. doi:10.1016/j.ijheatmasstransfer.2011.04.030.
26. Chien KH, Lin YT, Chen YR, Yang KS, Wang CC. A novel design of pulsating heat pipe with fewer turns applicable to all orientations. Int J Heat Mass Transf. 2012;55(21–22):5722–8. doi:10.1016/j.ijheatmasstransfer.2012.05.068.
27. Jun S, Kim SJ. Comparison of the thermal performances and flow characteristics between closed-loop and closed-end micro pulsating heat pipes. Int J Heat Mass Transf. 2016;95(1):890–901. doi:10.1016/j.ijheatmasstransfer.2015.12.064.
28. Jung C, Kim SJ. Investigation into the effects of passive check valves on the thermal performance of pulsating heat pipes. Int J Heat Mass Transf. 2023;204:123850. doi:10.1016/j.ijheatmasstransfer.2023.123850.
29. Dixit T, Authelet G, Mailleret C, Gouit F, Stepanov V, Baudouy B. High performance and working stability of an 18 W class neon pulsating heat pipe in vertical/horizontal orientation. Cryogenics. 2023;132(1):103670. doi:10.1016/j.cryogenics.2023.103670.
30. Pei Z, Koito Y. Fluid distributions and flow characteristics in a polymer pulsating heat pipe: visualization experiments using HFE as a working fluid. In: Proceedings of the 33rd International Symposium on Transport Phenomena, 2023 Sep 24–27; Kumamoto, Japan.

31. Hideyama F, Koito Y. Heat transfer characteristics of an ABS polymer pulsating heat pipe fabricated by a 3-D printer. Therm Sci Eng. 2019;27(2):59–66.
32. Peng H, Pai PF, Ma H. Nonlinear thermomechanical finite-element modeling, analysis and characterization of multi-turn oscillating heat pipes. Int J Heat Mass Transf. 2014;69(8):424–37. doi:10.1016/j.ijheatmasstransfer.2013.10.041.